Proceedings of ASME:
Internal Combustion Engine Division
September, 2002, New Orleans

HEAT TRANSFER WITHIN DEFORMING DROPLETS

Meizhong Dai J. Blair Perot David P. Schmidt

University of Massachusetts-Amherst

ABSTRACT

The effect of droplet oscillation on internal heat transfer was investigated using a transient, three-dimensional Navier-Stokes solver for free-surface flows. The code solves conservation of momentum and energy on a three-dimensional deforming domain. The investigation sought to explore the effect that oscillations might have on temperature non-uniformity within droplets. Biot numbers of 0.1 and 0.25 were investigated for three different degrees of distortion: no perturbation, 13% and 35%. The droplets were given an initial perturbation and allowed to relax back to a spherical shape. The results show that the effect of the oscillation is minimal. As expected, the effect was greatest at large distortion and large Biot number. However, it appears that distortion does not contribute much to heat transfer within droplets.

INTRODUCTION

In diesel fuel injection, liquid drops initially start out cool and heat up as they encounter hot surrounding gasses and radiation heat transfer. The rate of heat transfer is important, because it helps to determine the rate of fuel evaporation. Thus, heat transfer to the droplets may be important to the mixture preparation and combustion.

During an initial heating-up period, evaporation is very slow, as shown in Fig. 1. The early heat transfer goes mostly into raising the temperature of the drop. Eventually, the surface reaches the wet-bulb temperature and the internal drop temperature approaches equilibrium. Once the initial heating-up period is completed, heat transfer proceeds much more rapidly [1].

In many cases, this heat transfer process may be analyzed by simply considering the droplet to be a lumped mass with a uniform internal temperature profile. However, in the case of especially high heat transfer, the lumped mass assumption may not be adequate. The inability to use the lumped mass assumption is inconvenient, because the general case requires a series solutions to the governing conduction equation.

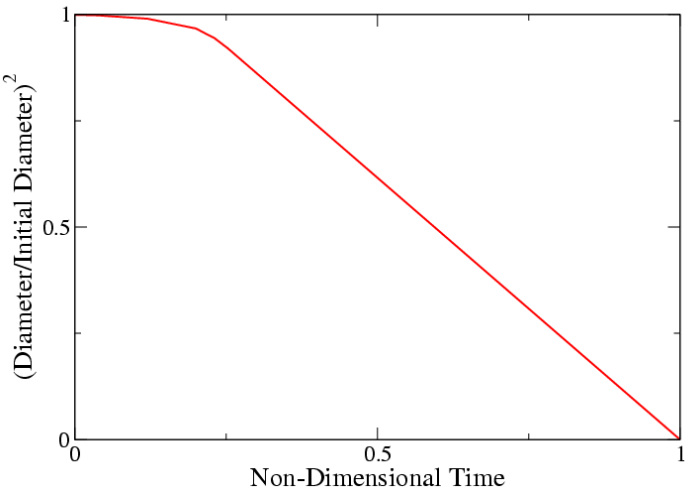

Figure 1. Drop size squared versus time for a typical evaporating drop [1].

However, droplets are generally not spherical or stationary. In the presence of external gas, the droplets may deform due to aerodynamic forces. Surface tension causes the drop shape to oscillate and viscosity damps the oscillation. This motion causes convection inside the drop and may help to distribute heat. If significant heat redistribution occurs, then the lumped mass assumption may be extended to higher rates of heat transfer, simplifying the modeling process.

The governing parameter is the Biot number, which represents the ratio of the rate of convection to internal conduction. The Biot number is defined as

$$Bi = \frac{h \cdot L_c}{k_l} \qquad (1)$$

The symbol h represents the convective heat transfer coefficient, L_c represents the droplet's characteristic length, and k_l is the liquid thermal conductivity. For a sphere, L_c is one-third the radius. At low Biot numbers, generally less than 0.1, the lumped mass assumption is adequate. At higher Biot numbers, the non-uniformity of the internal temperature profile significantly affects the heat flux at the droplet surface.

A few experimental and numerical efforts have investigated droplet internal heat transfer. Hader and Jog modeled a droplet suspended in a steady-state electric field [2]. The droplet assumed either an oblate or prolate shape, depending on the field and the surrounding fluid. The shape was deformed, but steady. Hader and Jog calculated the internal streamlines and heat transfer under these conditions. Wong and Lin made experimental measurements of internal drop temperatures [3]. They suspended 2mm diameter droplets in a high-temperature gas flow. By using 70 micron thermocouple junctions, they were able to observe internal temperature variations. They noted significant internal temperature variations that were dependent somewhat on the internal droplet circulation. Megaridis solved the two-dimensional axisymmetric Navier-Stokes equations and calculated internal droplet temperatures [4].

One feature of these experiments and calculations was that the drop shape did not change in time. However, droplets in real combustion applications are subjected to significant turbulent dispersion. Eddies accelerate droplets, likely causing significant droplet distortion. This distortion may have implications for droplet heating-up. The details of this acceleration and the coupling with droplet distortion are currently very difficult to calculate. However, simplified models are possible.

The present work will show if the lumped mass assumption can be used at Biot numbers above 0.1 due to droplet oscillation. Oscillation creates a mixing effect of internal convection. Additionally, oscillation temporarily increases the surface area of the drop. The spherical drop is a minimum possible surface area. This paper will calculate how internal heat transfer is promoted in oscillating droplets.

Temperature is modeled as a passive scalar that is convected and conducted in a deforming droplet. The surrounding gas motion is not currently calculated, but rather a uniform value of heat transfer coefficient is imposed on the droplet boundary. This simplification precludes the simulation of internal vortices, which would further promote internal temperature redistribution within the drop [5]. Instead, the droplet is given an initial perturbation that causes the droplet to oscillate. The results will indicate if the oscillatory motion is sufficient to promote additional heat transfer.

NUMERICAL METHOD

The numerical method used in this work is based on a stream-function formulation of the Navier-Stokes equations. The complete Navier-Stokes equations were solved in three dimensions on a deforming unstructured mesh. Though the current problem could be rendered in two dimensions, the three-dimensional approach avoids dealing with the mild singularity that occurs at a line of axisymmetry. The basic equations were solved for a deforming, moving, control volume, avoiding the interpolation errors inherent in global remeshing. The method has some common features with Arbitrary Lagrangian-Eulerian methods. However, the current approach is not a fractional step method.

Dai et al. [6] have provided more extensive information about this numerical scheme. The method uses an unstructured mesh, which allows maximum flexibility in matching mesh cells with the boundary surfaces. In three dimensions, the basic control volume is a tetrahedron. The basic parameter and real unknown is the stream function, which is a vector in 3 dimensional calculations.

Momentum equations can be developed after the velocities are obtained from the stream function. The procedure is complex since the mesh has to be moved in order to track the free surface. Beginning with the Reynolds transport theorem for incompressible flow, we have:

$$\frac{d}{dt}\int_{CV}\rho\mathbf{u}dv+\int_{CV}\nabla\cdot\rho\mathbf{u}(\mathbf{u}-\mathbf{v})dv=\int_{CV}\rho\mathbf{f}dv-\int_{CV}\nabla pdv+\int_{CV}\mu\nabla^2\mathbf{u}dv \tag{2}$$

where **f** is the body force, **v** is the mesh velocity, and *CV* is the control volume. Assuming the control volume is small enough, and the velocity **u** is linear within each of them, the integral form can be changed to:

$$\frac{1}{\Delta t}[(\rho\mathbf{u}V)^{n+1}-(\rho\mathbf{u}V)^n]+(\nabla\cdot\rho\mathbf{u}(\mathbf{u}-\mathbf{v})V)^n=(\rho\mathbf{f}V)^n-(\nabla pV)^{n+1}+(\mu\nabla^2\mathbf{u}V)^{n+1/2} \tag{3}$$

$$\frac{1}{\Delta t}[(\rho\mathbf{u})^{n+1}-(\rho\mathbf{u})^n\frac{V^n}{V^{n+1}}]+(\nabla\cdot\rho\mathbf{u}(\mathbf{u}-\mathbf{v}))^n\frac{V^n}{V^{n+1}}=(\rho\mathbf{f})^n\frac{V^n}{V^{n+1}}-(\nabla p)^{n+1}+(\mu\nabla^2\mathbf{u})^{n+1/2}\frac{V^{n+1/2}}{V^{n+1}} \tag{4}$$

where the parameters **u**, p, and ρ are defined at the center of each control volume, and n and n+1 represent different time steps. The value of the cell volume at the n+1 time step is predicted from the velocity at the n time step; therefore this is still a linear equation. Note that an implicit method, Crank-Nicolson differencing, is applied to develop implicit schemes for the diffusion terms. The divergence operators in the

convection and diffusion terms can be evaluated using Gauss' Divergence Theorem:

$$[\nabla \cdot \rho \mathbf{u}(\mathbf{u}-\mathbf{v})] = \frac{1}{V} \sum_{\text{cell faces}} \rho \mathbf{u}(\mathbf{u}-\mathbf{v}) \cdot \hat{\mathbf{n}} A_f \quad (5)$$

$$[\mu \nabla \cdot (\nabla \mathbf{u})] = \frac{1}{V} \sum_{\text{cell faces}} \mu \nabla \mathbf{u} \cdot \hat{\mathbf{n}} A_f \quad (6)$$

In the above equations, the gradient term in each cell can be calculated by least squares data fitting if the velocity is positioned at the cell's center of gravity. As a final step, the velocity **u** is expressed in terms of the stream function component $\mathbf{s} \cdot \mathbf{t}$ defined on each cell edge. Then Eqn. (3) is integrated on a closed path around the edges, producing the discrete equivalent of a curl operation. This results a set of equations for the stream function on each cell edge. These equations are solved for the moving, deforming cells.

Surface curvature is evaluated by fitting a parabolic surface to the neighborhood of a surface face. This method produces a second-order accurate estimate of the curvature. The surface tension force is included on the boundaries as an explicit term. The only disadvantage of this scheme is that the surface tension force integrated over the closed surface is not exactly zero due to numerical error. The center of mass drifts during the calculations due to this numerical error.

Internal temperature was calculated using the Reynolds transport theorem. For a passive scalar with constant transport properties, this is given by Eqn. (7). The only transport property of significance is the thermal diffusivity, α.

$$\frac{d}{dt} \int_{CV} T dv + \int_{CV} \nabla \cdot T(\mathbf{u}-\mathbf{v}) dv = - \int_{CV} \alpha \nabla^2 T dv \quad (7)$$

This equation is solved consistently with the method used for the momentum equations. The boundary condition on the transport equation is given by Eqn. (8).

$$-k \frac{\partial T}{\partial x} = h(T - T_\infty) \quad (8)$$

The temperatures are non-dimensionalized to range from zero to unity. The value of T_∞ is set to zero and the initial temperature in the droplet is unity.

VALIDATION

In order to validate the numerical scheme, the oscillation of an initially spherical drop was calculated. By using a very small initial distortion, the results could be compared to the theoretical small-perturbation solution from Lamb [7]. As an initial condition, the following three-dimensional, axisymmetric velocity field was used.

$$v_x = x \quad (9)$$

$$v_y = y \quad (10)$$

$$v_z = -2z \quad (11)$$

This perturbation causes the spherical drop to oscillate between an oblate and prolate spheroid shape. According to Lamb [7] the drop oscillation period for an infinitesimal, mode 2 perturbation is:

$$T = 2\pi \frac{1}{\sqrt{n(n-1)(n+2)\frac{\sigma}{\rho r_0^3}}} = 2\pi \frac{1}{\sqrt{8\frac{\sigma}{\rho r_0^3}}} \quad (12)$$

These preliminary calculations were performed using a mesh of 4,500 cells. The calculated ratio between the largest diameter and the undisturbed drop diameter is shown in Figure 2. Note that the shape is non-sinusoidal for two reasons. As the droplet passes from oblate to prolate, the direction of the largest diameter switches from the *z*-axis to a plane perpendicular to the *z*-axis. In addition, due to conservation of mass and the axisymmetric nature of the flowfield, the prolate distortion is twice the oblate distortion.

The distortion can be used to judge the period of oscillation. In Figure 2, the theoretical period as predicted by Eqn. (12) is marked with a vertical line. The agreement is excellent. The small amount of error is due to two sources: numerical error and the finite amplitude of the imposed disturbance. Regardless, the accuracy of the method is satisfactory for an oscillating drop.

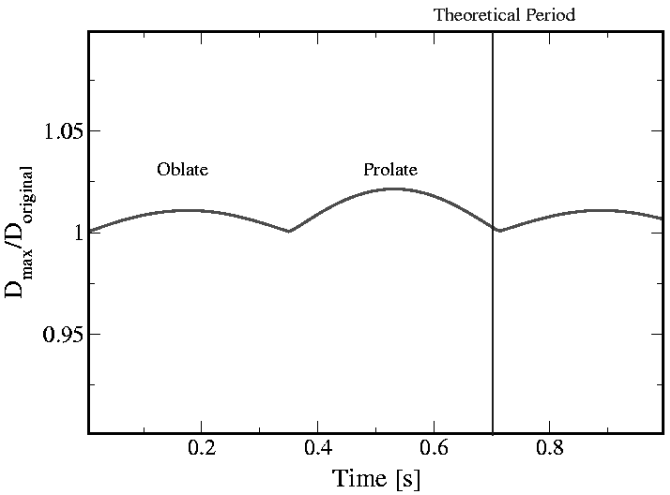

Figure 2. Oscillation of a droplet subject to a small disturbance.

For the heat transfer calculations, a much larger distortion was used. The shape of the deforming drop is shown in Figures 3 and 4. This figure is taken from the prolate part of the oscillation. The figure also shows the adaptation of the mesh to the drop shape and the spatial variation in the z velocity.

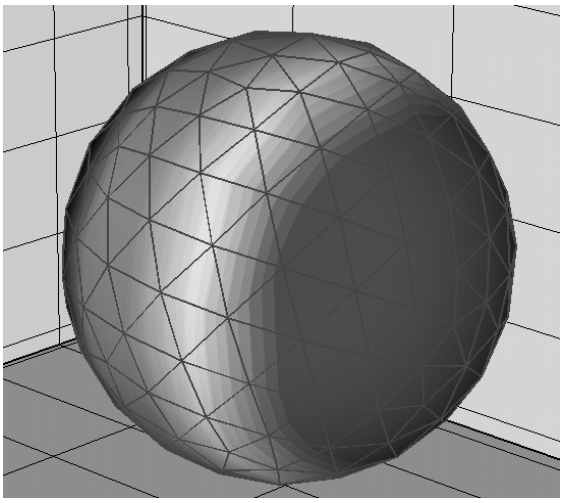

Figure 3. The initial state of a droplet. The droplet surface is shaded by the z component of velocity.

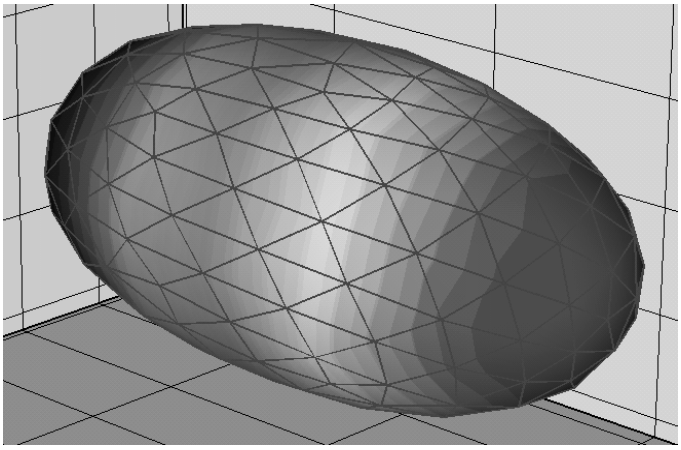

Figure 4. The distorted droplet. The droplet surface is shaded by the z component of velocity.

RESULTS

The drops in most combustion applications are rapidly exposed to high temperatures. The fuel may already be warmed by the time it is injected. As a reasonable approximation of typical fuel conditions, the liquid properties were set according to diesel fuel at a temperature of 500K. The properties were treated as constant for the sake of this investigation.

In order to validate the code's heat transfer calculations, a case was run with no fluid motion. The stationary droplet case is equivalent to conduction in a sphere. For a sphere initially at a uniform temperature and subject to a uniform convective heat transfer boundary condition, the analytical solution is given by a series solution [8].

$$\theta = \sum_{n=1}^{\infty} C_n \exp(-\zeta_n^2 Fo) \frac{1}{\zeta_n r^*} \sin(\zeta_n r^*) \tag{13}$$

where: $r^* = r / r_0$, $Fo = \frac{t\alpha}{r_0^2}$, $C_n = \frac{4[\sin(\zeta_n) - \zeta_n \cos(\zeta_n)]}{2\zeta_n - \sin(2\zeta_n)}$

and the values of ζ_n are positive roots of the transcendental equation:

$$1 - \zeta_n \cot(\zeta_n) = Bi = \frac{hr_0}{k_l} \tag{14}$$

Figure 5 shows a comparison of the computed and analytical solution of the internal temperature profile. The data are at a non-dimensional time of 0.08. Time is non-dimensionalized using the thermal diffusivity and characteristic length to form the Fourier number.

$$Fo = \frac{t\alpha}{L_c^2} \tag{15}$$

The temperature is scaled from zero to unity based on the initial temperature, T_0, and the ambient temperature, T_∞. The non-dimensional temperature is denoted as θ.

$$\theta = \frac{T - T_\infty}{T_0 - T_\infty} \tag{16}$$

For all the heat transfer calculations, ten thousand cells were used. Because the cells are tetrahedral, the radial locations of nodes are not uniformly distributed from zero to the drop radius, R. For example, there are no nodes that lie exactly at r=0. To combine all the data into a two-dimensional plot, nodes were grouped by radial location into "bins." The plots that follow represent the average value for each bin versus the radial location of the bin. Because of this method of compilation, the curves are not necessarily smooth.

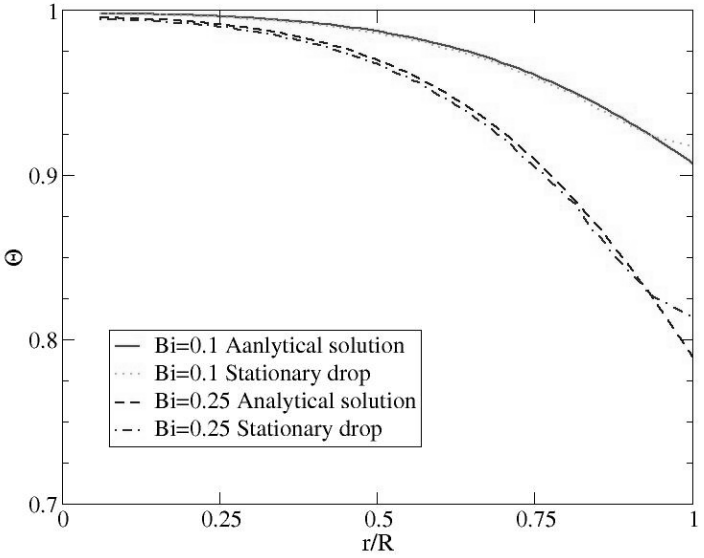

Figure 5. Validation of the calculations against analytical solutions. This is a plot of non-dimensional temperature versus non-dimensional radius at a non-dimensional time of 0.08.

Figure 5 shows the results for a stationary droplet. The Biot number in Fig. 5 is 0.1 and 0.25. Note the significant inhomogeneity in the temperature. As expected, the larger the Biot number, the greater the degree of inhomogeneity. The computed results agree well with the analytical solution, with a tolerable amount of numerical error. The temperature gradients that occur at the drop interface are likely to be to blame: they are initially very steep, and not easily resolved.

For oscillating drops, two Biot numbers and three levels of distortion were investigated. Distortion is quantified by measuring the distance from the center of mass to the point on the surface that is furthest away. The distortion is non-dimensionalized by the undisturbed drop radius. The two Biot numbers were 0.1 and 0.25. The three levels of distortion were 0%, 13% and 35%. Consequently, there are six cases (two Biot numbers times three distortions) to be considered. For the two levels of distortion, the initial velocities are different. These are used to calculate the initial Reynolds number and Weber number, as shown in Table 1. The Prandtl number, which only depends on fluid properties, was equal to 7.8 for all cases.

Initial Distortion Velocity (m/s)	Weber Number	Reynolds Number
0.10	0.0764	28.86
0.25	0.4775	72.15

Table 1. Initial Weber number and Reynolds number based on characteristic length and initial distortion velocity.

To quantify the effect of an initial disturbance, the droplet was simulated until a significant amount of energy transfer had occurred. To compare the radial temperature distribution to that of an undisturbed drop, the data needed to be taken from a spherical drop. Twice during each period of oscillation, the droplet passes through a spherical shape. It was found that at a non-dimensional time of (Fourier number) of 0.055, such a spherical shape occurred. This was used as a reference point for the remaining plots. Figure 6 shows the distortion versus Fourier number for the low-distortion calculations. Since the properties were treated as constant, the oscillations were independent of Biot number. Note that the oscillations are of the same form seen in Fig. 2. The droplet alternates between an oblate and prolate shape. Since the maximum diameter is used, regardless of direction, to quantify distortion, the distortion is always greater than unity. Figure 6 also clearly shows the effect of viscous dissipation. Similar results are plotted in Figure 7 for the large-distortion case. After a Fourier number of 0.07, the droplet is nearly spherical and stationary.

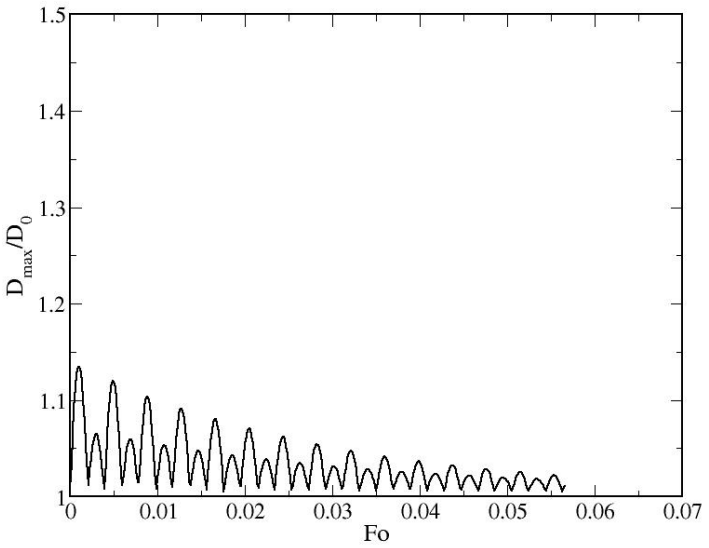

Figure 6. The distortion versus non-dimensional time (Fourier number) for an initial disturbance of 13%.

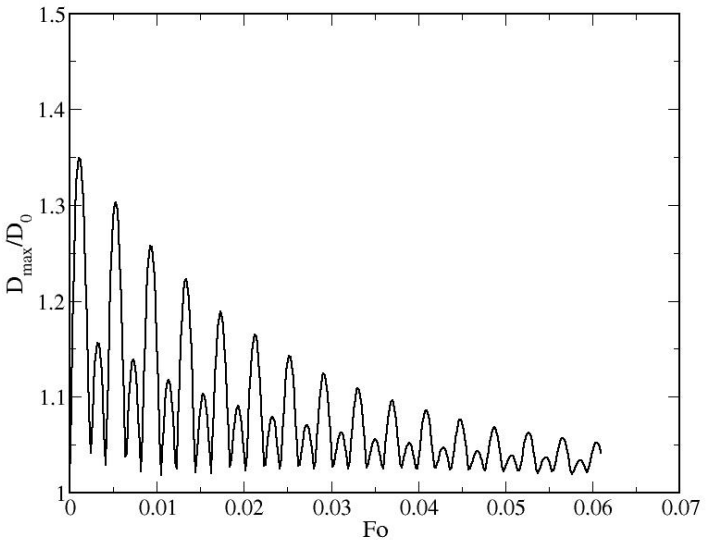

Figure 7. The distortion versus non-dimensional time (Fourier number) for an initial disturbance of 35%.

The temperature profiles were recorded for each of the six cases at a Fourier number of 0.055. The three cases of Biot number of 0.1 were compared to each other and are plotted in Figure 8. As expected, at this Biot number the temperatures are fairly uniform, regardless of the distortion magnitude. One interesting result is that the shape of the temperature profile is not significantly altered by the convection in the distorting drop or by its increased surface area.

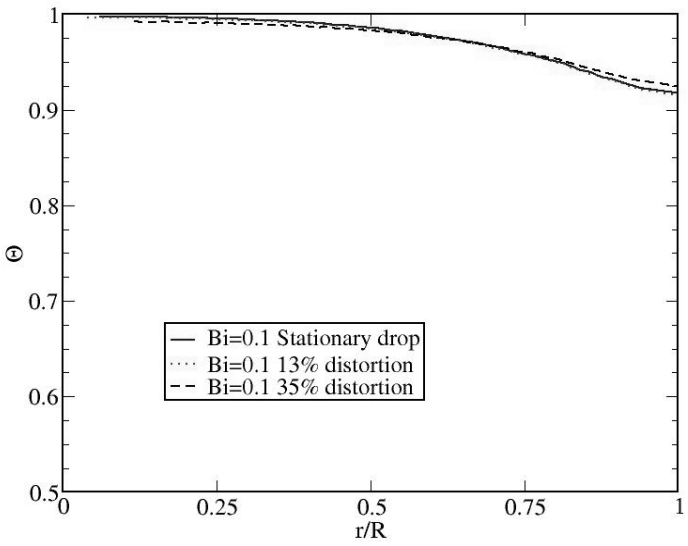

Figure 8. Temperature profiles in a droplet at Fo=0.055. All three cases are at a Biot number of 0.1.

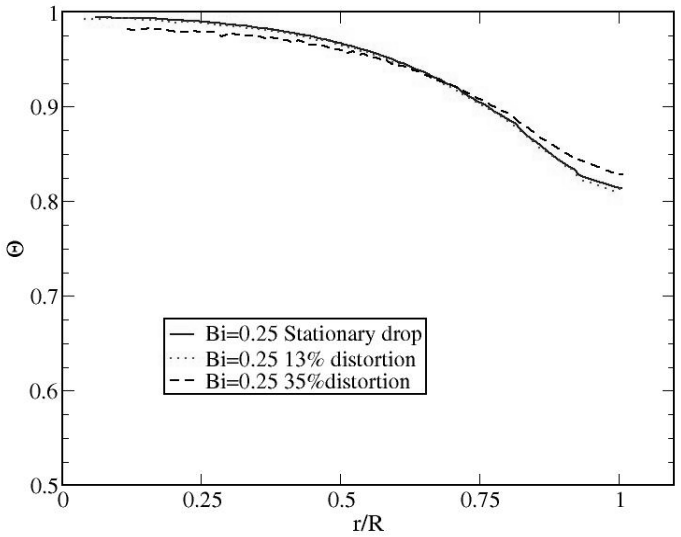

Figure 9. Temperature profiles in a droplet at Fo=0.055. All three cases are at a Biot number of 0.25.

Figure 9 shows similar results, but for a higher Biot number. When the Biot number is higher, internal conduction is slower and one expects greater temperature variations within the drop. This is indeed the case in Fig. 9. The oscillation of the drop also produces slightly more of an effect than in the lower Biot number case. The increased sensitivity to the oscillation is expected, since internal resistance to conduction is greater at larger Biot number, and convection is an enhancement to heat transfer. As expected, the large distortion produces a more uniform temperature profile than occurs in the stationary case. Nevertheless, Fig. 9 shows that the impact of the distortion is small. The large distortion temperature profile is very near that of the zero distortion profile.

CONCLUSIONS

A numerical model has been used to investigate the effect of droplet oscillation on internal heat transfer. The working hypothesis was that droplet oscillation would make the temperature within oscillating droplets more uniform. This trend was observed, however the magnitude of the effect was very small. Consequently, the effect of droplet distortion on internal heat transfer can be neglected for Biot number less than 0.25 and initial distortions less than 35%. It should be noted that the case investigated here was for a droplet subject to an initial perturbation and then allowed to stabilize. The effect of oscillations might be greater in a drop subject to continuous perturbations, such as in turbulent flow. In addition, an irrotational perturbation was used in this work. Other types of perturbation might promote greater mixing.

ACKNOWLEDGMENTS

This work was funded in part by an Office of Naval Research Young Investigator Grant under the supervision of Dr. Gabriel Roy.

REFERENCES

[1] Lefebvre, Arthur H., *Atomization and Sprays*, 1989, Hemisphere Publishing Corporation

[2] Hader, M. A. , Jog, M. A., Effect of Drop Deformation on Heat Transfer to a Drop Suspended in an Electrical Field, *Journal of Heat Transfer-Transactions of the ASME*, 120 (3): 682-689 Aug 1998

[3] Wong, S. C., Lin, A. C., Internal Temperature Distributions of Droplets Vaporizing in High-Temperature Convective Flows, *Journal of Fluid Mechanics*, 237: 671-687 Apr 1992

[4] Megaridis, C. M., Comparison Between Experimental Measurements and Numerical Predictions of Internal Temperature Distributions of a Droplet Vaporizing Under High-Temperature Convective Conditions, *Combustion and Flame*, 93 (3): 287-302 May 1993

[5] Faeth, G. M. 1977 Current Status of Droplet and Liquid *Combustion. Prog. Energy & Combust.* Sci. 3, 191-224.

[6] Dai, M., Wang, H., Perot, J. B., and Schmidt, D. P., Direct Interface Tacking of Droplet Deformation, *Atomization and Sprays*, to be published

[7] Lamb, H., *Hydrodynamics*, 1945, 6th edition, Dover Publications, Inc.

[8] Incropera, F. P., and Dewitt, D. P., *Fundamentals of Heat and Mass Transfer*, 5th edition, 2001, John Wiley & Sons